

Anti-neuroinflammatory effects of *Ephedra sinica* *Stapf* extract-capped gold nanoparticles in microglia

This article was published in the following Dove Press journal:
International Journal of Nanomedicine

Sun Young Park¹
Eun Hye Yi²
Yoon Kim²
Geuntae Park³

¹Bio-IT Fusion Technology Research Institute, Pusan National University, Busan, Republic of Korea; ²HYUNDAI ENTEC Research Institute, HYUNDAI ENTEC, Busan, 46048, Republic of Korea; ³Department of Nanofusion Technology, Graduate School, Pusan National University, Busan, Republic of Korea

Background: Combination therapy remains a promising strategy for treating neurodegenerative diseases, although green synthesis of gold nanoparticles for treating chronic neuroinflammation and studying their efficacy in treating neuroinflammation-mediated neurodegenerative diseases is not well assessed.

Results: Here, *Ephedra sinica* *Stapf* (ES) extract was used as the reducing, capping, and stabilizing agent for gold nanoparticle synthesis. We developed ES extract-capped gold nanoparticles (ES-GNs) and investigated their anti-neuroinflammatory properties in microglia. ES-GNs displayed maximum absorption at 538 nm in ultraviolet-visible spectroscopy. Dynamic light scattering assessment revealed that ES-GN diameter was 57.6±3.07 nm, with zeta potential value of -24.6±0.84 mV. High resolution-transmission electron microscopy confirmed the spherical shape and average diameter (35.04±4.02 nm) of ES-GNs. Crystalline structure of ES-GNs in optimal conditions was determined by X-ray powder diffraction, and elemental gold presence was confirmed by energy-dispersive X-ray spectroscopy. Fourier transform-infrared spectroscopy confirmed gold nanoparticle synthesis using ES. Anti-neuroinflammatory properties of ES-GNs on production of pro-inflammatory mediators (nitric oxide, prostaglandin E₂, and reactive oxygen species) and cytokines (tumor necrosis factor- α , IL-1 β , and IL-6) in lipopolysaccharide (LPS)-stimulated microglia were investigated by ELISA and flow cytometry. ES-GNs significantly attenuated LPS-induced production of pro-inflammatory mediators and cytokines, which was related to suppressed transcription and translation of inducible nitric oxide synthase and cyclooxygenase-2, determined by RT-PCR and western blotting. ES-GNs downregulated upstream signaling pathways (I κ B kinase- α/β , nuclear factor- κ B, Janus-activated kinase /signal transducers and activators of transcription, mitogen-activated protein kinase, and phospholipase D) of pro-inflammatory mediators and cytokines in LPS-stimulated microglia. Anti-neuroinflammatory properties of ES-GNs were mediated by ES-GNs-induced AMP-activated protein kinase-mediated nuclear erythroid 2-related factor 2 /antioxidant response element signaling.

Conclusion: Collectively, these findings provide a new insight on the role of ES-GNs in treating chronic neuroinflammation-induced neurodegenerative diseases.

Keywords: gold nanoparticle, *Ephedra sinica* *Stapf*, microglia, neuroinflammation

Correspondence: Geuntae Park
Department of Nanofusion Technology,
Graduate School, Pusan National
University, Busan 609-735, Republic of
Korea
Tel +8 251 510 3740
Fax +8 251 518 4113
Email gtpark@pusan.ac.kr

Sun Young Park
Bio-IT Fusion Technology Research
Institute, Pusan National University, Busan
46241, Republic of Korea
Tel +8 251 510 3631
Fax +8 251 514 7065
Email sundeng99@pusan.ac.kr

Introduction

Advances in nanotechnology allow the production of biocompatible nanoparticles with “green” synthesis techniques. Among the nanomaterials, gold nanoparticles can be synthesized with great precision using medicinal plants.^{1,2} Furthermore, medicinal plants are the most effective and high-performance reducing, capping,

and stabilizing agents because their reducing, capping, and stabilizing capacity direct the synthesis of gold nanoparticles and enables well-programmed tuning of nanoscale materials.^{3–5} Gold nanoparticles synthesized from medicinal plants provide unprecedented opportunities in a number of environmental and biomedical applications, including use as anti-inflammatory, anti-cancer, and anti-angiogenic agents and for drug/gene delivery.^{6,7} The unique advantages of “green” synthesis over conventional chemical synthesis can be straightforwardly and rapidly exploited for biomedical materials. Owing to the “green” synthesis of biocompatible gold nanoparticles, which do not yield hazardous environmental waste by-products, they have drawn attention as a useful bionanomaterial with the emergence of bionanotechnology.^{8–10} Therefore, the aim of this study was to contribute to the discovery and identification of biocompatible gold nanoparticles synthesized with *Ephedra sinica* Stapf (ES) against neuroinflammatory-mediated neurodegenerative diseases, including frontotemporal dementia and amyotrophic lateral sclerosis as well as Alzheimer, Huntington, and Parkinson disease.

Neuroinflammation, inflammation of the central nervous system (CNS), has recently been recognized to play key roles in the pathogenesis of neurodegenerative disorders. In addition, neuroinflammation, characterized by chronic activated microglia, can lead to neuronal damage and often results from its dysfunction.^{11,12} Microglia are one of the resident immune cells of the brain that maintain CNS homeostasis by clearing neuronal damaged cells and debris. In their quiescent state in healthy condition, microglia monitor the neighboring environment with their extensive processes.^{13,14} Nevertheless, upon recognizing a disruption in homeostasis, microglia activate the production of cytokines, such as tumor necrosis factor- α (TNF- α), IL-1 β , IL-6, and inflammatory mediators, including ROS, nitric oxide (NO), prostaglandin E₂ (PGE₂), inducible nitric oxide synthase (iNOS), and cyclooxygenase (COX)-2. The stage of neuroinflammation in neurodegenerative diseases is correlated with the generation of TNF- α , IL-6, ROS, NO, and PGE₂, whose circulating levels are typically evaluated in chronic neuroinflammation. These mediators and cytokines play pivotal roles in the promotion of neurodegenerative disorders.^{15,16} As mentioned above, neuroinflammatory mediators and cytokines play an imperative role as a messenger in homeostatic functions of microglia, but their persistent or prolonged production from chronic-activated microglia plays a pivotal role in chronic neuroinflammatory-mediated neuropathogenesis

and serves as a prolific factor of neurodegenerative disorders.^{17,18} Therefore, the discovery of biocompatible gold nanoparticles with anti-neuroinflammatory activity that could limit possible neuroinflammatory-mediated neurodegenerative diseases is desired.

A high number of intracellular signaling major pathways, including I κ B kinase (IKK)- α/β , nuclear factor-kappa B (NF- κ B), Janus-activated kinase (JAK)/signal transducers and activators of transcription (STAT), mitogen-activated protein kinase (MAPK), and phospholipase D (PLD) signaling pathways, participate in neurodegenerative disorders and lead to the production and expression of stimulatory pro-inflammatory-inducible enzymes.^{19,20} Moreover, IKK- α/β -NF- κ B signal contains p50/p65; p50/p65 forms a complex with I κ B α in the cytosol and then releases p50/p65 that is translocated to the nucleus where it regulates the transcription of COX-2, iNOS, TNF- α , IL-1 β , and IL-6. Moreover, the JAK/STAT signal also plays an important role in the activation of microglia and leads to the upregulation of these pro-inflammatory inducible enzymes and cytokine expression.^{21,22} Notably, lipopolysaccharide (LPS), a well-known endotoxin of the outer membrane of Gram-negative bacteria, induces neuroinflammation, and IKK- α/β -NF- κ B and JAK/STAT signaling are critical for promoting neurodegenerative disorders. However, microglia inhibitors or small interfering (si)RNA system of IKK- α/β -NF- κ B and JAK/STAT signaling have been reported to suppress neuroinflammatory-mediated neurodegenerative diseases.^{23,24}

AMP-activated protein kinase (AMPK) and nuclear erythroid 2-related factor 2 (Nrf2) are the two modulators of anti-inflammatory mechanism that are involved in the regulation of neuronal cell defense and repair systems. AMPK is a master regulator of energy homeostasis and mediates anti-inflammatory mechanism by activation of Nrf2 signal.^{25,26} Moreover, AMPK inhibits LPS-mediated activation of IKK- α/β -NF- κ B and JAK/STAT signaling in microglia and macrophages. Activation of Nrf2 and nuclear translocation leads to transcriptional activation of antioxidant responsive element (ARE), which regulates anti-inflammatory genes, such as heme oxygenase-1 (HO-1) and NAD(P)H:quinone oxidoreductase (NQO1). AMPK mediates Nrf2/ARE signaling, leading to the transcription activity of Nrf2, and then induces anti-inflammatory genes. Importantly, AMPK and Nrf2 signaling are highly interconnected.^{27,28} Together they regulate many genes involved in neurodegenerative disorders. Studies have shown that neuroinflammation promotes neurodegenerative

disorders, and AMPK and Nrf2 play important roles in the development of neurodegenerative disorders. Nrf2 is also an anti-inflammatory factor of neurodegenerative disorders and upregulates the expression of anti-inflammatory mediators, HO-1 and NQO1, and decreases the expression of pro-inflammatory mediators, iNOS and COX-2. HO-1 and NQO1, well-known intracellular-inducible Phase II enzymes, regulate neurodegenerative disorders. Accumulating evidence has indicated that Nrf2-mediated HO-1 and NQO1 activation suppresses production of pro-inflammatory mediators and cytokines and plays roles in an array of biological processes, including alleviation of symptoms of neuroinflammation-mediated neurodegenerative diseases.^{24,29,30}

ES, commonly known as Ephedra or Ma Huang, is native to central Asia. It has been commonly used as an anti-inflammatory agent and to treat autoimmune diseases, including pyrexia, asthma, and rheumatoid arthritis, in Traditional Chinese Medicine.³¹ Recently, studies have indicated that ES can target the CNS and can mitigate ischemic brain injury. ES extract exhibits antioxidant, anti-inflammatory, anti-arthritis, anti-obesity, and neuroprotection effects.^{32–36} Based on the wide range of bioactivities of ES as mentioned above, we supposed that it may be a good “green” candidate for the preparation of ES extract-capped gold nanoparticles (ES-GNs) with potential pharmacological effects.

Therefore, in this study, we aimed to explore the advantages of green synthesis of ES-GNs, which were characterized for its physicochemical properties by ultraviolet-visible (UV-Vis) spectrometry, dynamic light scattering (DLS), high resolution-transmission electron microscopy (HR-TEM), energy-dispersive X-ray spectroscopy (EDS), X-ray powder diffraction (XRD), and Fourier transform-infrared spectroscopy (FT-IR). Furthermore, we evaluated the effects of ES-GNs in interlink of neuroinflammation–neurodegenerative disorders; the results showed that pro-inflammatory mediators and cytokines were downregulated by ES-GN treatment. Moreover, ES-GNs suppressed activation of a variety of neuroinflammation signaling pathways, such as IKK- α/β –NF- κ B, JAK/STAT, and MAPK, and subsequently decreased either the downstream target mediators of these signaling pathway or cytokines in LPS-stimulated microglia. Intriguingly, ES-GNs failed to weaken chronic-activated microglia by knockdown of AMPK, Nrf2, HO-1, and NQO1, indicating that the beneficial effects of ES-GNs on regulation of neuroinflammation were dependent on the AMPK–Nrf2 signaling pathway. These findings provide a new insight on the application of ES-GNs in

neuroinflammation-mediated neurodegenerative disorders and may help confine the effects of chronic-activated microglia to neurodegenerative diseases.

Material and methods

Materials and chemicals

Analytical grade reagents of DPPH (2,2-diphenyl-1-picrylhydrazyl), ABTS [2,2'-azino-bis (3-ethylbenzothiazoline-6-sulphonic acid)], chloroauric acid [$\text{HAuCl}_4 \cdot 3\text{H}_2\text{O}$; also known as gold(III) chloride], MTT, LPS from *Salmonella enterica*, X-tremeGENE siRNA, FuGENE HD transfection reagents, and other reagents were supplied by Sigma-Aldrich (St. Louis, MO, USA) and used as received. A Cytotoxicity Detection kit for determining lactate dehydrogenase content (LDH) was procured from Roche Applied Science (Rotkreuz, Switzerland). The chloromethyl derivative of H2DCFDA (CM-H2DCFDA) was supplied by Thermo Fisher Scientific Inc. (Waltham, MA, USA). Mouse TNF- α , IL-1 β , and IL-6 Quantikine ELISA kits were obtained from R&D Systems Inc. (Minneapolis, MN, USA). Primary antibodies against TBP, α -tubulin, iNOS, extracellular signal-regulated kinases (ERK), c-Jun N-terminal kinase (JNK), p38, HO-1, COX-2, Nrf2, I κ B α , NF- κ Bp65, and NQO1 were sourced from Santa Cruz Biotechnology (Santa Cruz, CA, USA). Antibodies against p-glycogen synthase kinase 3 beta (GSK-3 β), GSK-3 β , p-p65, p-I κ B α/β , I κ B α/β , p-I κ B α , I κ B α , STAT-1, p-STAT-1, p-ERK, p-38, p-JNK, JAK, p-JAK1, p-AMPK, and AMPK were obtained from Cell Signaling Technology (Beverly, MA, USA). siRNAs specific for mouse AMPK, HO-1, Nrf2, and NQO-1 were sourced from Santa Cruz Biotechnology.

Total phenol content assay of ES extract

The Folin–Ciocalteu colorimetric method was used for the assessment of total phenol content in ES extract³⁷ with some modifications. ES extract was incubated for 2 mins with Folin–Ciocalteu reagent, and then 0.708 mol/L Na_2CO_3 was added. The mixture was incubated at room temperature (22–25°C) for 2 hr, and absorbance was quantified at 700 nm using Ultrospec 6300 Pro (GE Healthcare Life Sciences, Buckinghamshire, UK). The results were expressed as gallic acid equivalent per gram ES extract.

Total flavonoid content assay of ES extract

The aluminum chloride colorimetric method was used for determination of total phenol content of ES extract³⁸ with

some modifications. ES extract was mixed with an equal volume of double distilled water, followed by addition of 5% NaNO₂. After incubating at room temperature for 5 mins, 10% AlCl₃ was added to the mixture, incubated at room temperature for 5 mins, and 1 M NaOH was added to the mixture. Absorbance was analyzed at 510 nm using the VICTOR Multilabel Plate Reader (Perkin-Elmer, Waltham, MA, USA). The total flavonoid content was expressed as microgram quercetin equivalent per gram ES extract.

DPPH free radical scavenging assay of ES extract

DPPH free radical scavenging activity of ES extracts was determined according to a previously described method³⁹ with some modifications. Equal volumes of 60 μM DPPH solution and ES extract were mixed in microplates. The mixture was allowed to stand for 30 mins at room temperature (22–25°C) in the dark, and absorbance was analyzed at 510 nm using the VICTOR Multilabel Plate Reader.

ABTS radical scavenging assay of ES extract

ABTS radical scavenging activity of ES extracts was analyzed following a previously reported method⁴⁰ with slight modifications. Stock solutions of 7 mM ABTS and 2.6 mM potassium persulfate were prepared in double distilled water at room temperature (22–25°C) in the dark for 16 hrs. ES extracts were mixed with the working solution and then allowed to stand for 30 mins at room temperature (22–25°C) in the dark. Absorbance was quantified at 734 nm using Ultrospec 6300 Pro (GE Healthcare Life Sciences).

Assaying reducing power of ES extract

Reducing power potential of ES extract was determined following a previously described method.³⁸ Serial dilution of ES extract was performed in 0.2 M phosphate buffer (pH 6.6) containing 1% potassium ferric cyanide. The mixture was incubated at room temperature (22–25°C) for 20 mins. Next, 10% trichloroacetic acid was added to this mixture and centrifuged (3000×g) for 10 mins. The supernatant was mixed with 0.1% ferric chloride, and absorbance was quantified at 700 nm with Ultrospec 6300 Pro (GE Healthcare Life Sciences). Ascorbic acid was used as the standard, and results were expressed as microgram ascorbic acid equivalents per gram sample.

Green synthesis of ES-GNs

ES stem was purchased from Kwang Myoung Herb Medicine (Busan, South Korea) in September 2016. To prepare ES extract, chopped ES stem was extracted in distilled water at 100°C for 4 hrs. ES supernatant was vacuum-filtered (0.45-μm pore size filter; Sartorius Biotech GmbH, Gottingen, Germany), freeze-dried (final yield of 27 g), and stored in a refrigerator (4°C). ES freeze-dried extract was dissolved in distilled water and filter-sterilized through a 0.22-μm pore filter (Sartorius Biotech GmbH, Gottingen, Germany) and stored in a refrigerator (4°C). For the green synthesis of ES-GNs, a mixture of a 1 mM chloroauric acid solution and ES extract (2 mg/mL) was added under rigorous stirring (the mixture immediately turned violet) and was stationary incubated at room temperature (22–25°C) for 10 mins. Then, the remaining residues were eliminated by centrifugation at 13,000 rpm for 20 mins. ES-GNs were synthesized using the abovementioned procedure but without the addition of chloroauric acid.

Physicochemical characterization of ES-GNs

UV-Vis absorbance of ES-GNs was determined using Ultrospec 6300 Pro (GE Healthcare Life Sciences). DLS and zeta-potential measurements of ES-GNs were performed on the Zetasizer Nano ZS90 (Malvern Instruments, Malvern, UK). HR-TEM and EDS studies were performed using a TALOS F200X HR-TEM operated at an accelerating voltage of 200 kV and equipped with a dispersive X-ray spectroscopy. XRD measurements were recorded using an X-ray diffractometer (XRD Empyrean series 2, PANalytical, Almelo, The Netherlands). The XRD pattern was determined with the following parameters: scanning range, 30–80; voltage, 40 kV; and current, 30 mA. FT-IR spectroscopy of ES extract and ES-GNs was performed using a FT-IR spectrophotometer (Spectrum GX, PerkinElmer, Inc., Boston, MA, USA) in the range between 4,000 and 400 cm⁻¹.

Isolation of mouse peritoneal macrophages and cell culture

Ethical statements: Guidelines for animal welfare as recommended by the National Institutes of Health Guide for the Care and Use of Laboratory Animals were followed. Entire experimental procedures were approved beforehand by the Institutional Animal Care and Use

Committee of the Pusan National University (Certification No. PNU-2017–1518). Isolated mouse primary microglia cultures were prepared as previously explained.⁴¹ The purity of microglia (>95%) was determined using anti-CD11b antibody by flow cytometer analysis. Briefly, mouse primary microglia were extracted from the frontal cortices of newborn (3-day-old) ICR mouse pups (Doo Yeol Biotech, Seoul, Korea). The isolated mixed glia were maintained in Dulbecco's Modified Eagle's Medium (DMEM)/F12 containing 20% FBS, 0.1 mM nonessential amino acids, 1 mM sodium pyruvate, 2 mM L-glutamine, and 50 mg/mL penicillin/streptomycin in poly-L-lysine-coated flasks at 37°C in a humidified atmosphere of 5% CO₂ and 95% air. After 2 weeks of culture, the mixed glia cells were shaken on an orbital shaker at 180 rpm, and the medium was then harvested. Primary microglia were subplated and used for further experiments. Mouse BV-2 microglial cells were maintained in DMEM (Welgene) with 5% heat-inactivated FBS and 1% penicillin/streptomycin solution (Welgene) at 37°C in a humidified incubator with 5% CO₂.

Cell viability measurement by MTT and LDH assay

For MTT assay, MTT solution was added to the remaining primary microglial and BV-2 microglial cell suspensions and incubated at 37°C for 4 hrs. Absorbance was analyzed at 570 nm using the VICTOR Multilabel Plate Reader. For determining extracellular LDH activity in primary microglial and BV-2 microglial cell culture media, we used a cytotoxicity detection kit according to the manufacturer's protocol. Absorbance was quantified at 490 nm using the VICTOR Multilabel Plate Reader.

Bioassay of NO and PGE₂ concentration

The supernatant of BV-2 microglial cells from each sample was collected for detecting the concentration of NO and PGE₂ with Griess Reagent System (Promega, USA) and Quantikine ELISA Kits according to the manufacturer's instructions. NO and PGE₂ concentration were detected at 540 and 490 nm, respectively, on the VICTOR Multilabel Plate Reader.

Cytokine assay for TNF- α , IL-1 β , and IL-6

Pro-inflammatory cytokines were quantified from cell-free culture supernatant using mouse TNF- α , IL-1 β , and IL-6 Quantikine ELISA kits. In brief, cultured primary

microglia and BV-2 microglial cells were pretreated with ES-GNs for 1 hr before treatment and with LPS for additional 24 hrs.

Total RNA and cDNA preparation for quantitative real-time PCR

Total RNA was extracted using QIAGEN RNeasy® Mini kit (QIAGEN GmbH, Germany), and cDNA was synthesized using Maxime RT PreMix (Bioneer, Daejeon, Korea) according to the manufacturer's protocol. Quantitative real-time PCR was performed using SYBR® Green Real-Time PCR Master Mixes (Thermo Fisher Scientific, Inc.) and Chromo4 RT-PCR detection system (Bio-Rad Laboratories, Inc., Hercules, CA, USA) according to the manufacturer's instructions. The relative gene expression was analyzed using the critical threshold method in Opticon Monitor software program.

Assay for PLD activity

PLD activity was quantified using Amplex Red PLD assay kit according to the manufacturer's protocol. In brief, cultured BV-2 microglial cells were pretreated with ES-GNs for 1 hr before an additional treatment with LPS for 24 hrs. PLD activity was observed indirectly using 10-acetyl-3,7-dihydroxyphenoxazine. The red fluorescence was quantified using the VICTOR Multilabel Plate Reader.

Transient transfection and dual luciferase activity assay

BV-2 microglial cells were cultured and then transfected with iNOS, NF- κ B, COX-2, ARE, or HO-1-luc reporter plasmids (containing the firefly luciferase gene) using the FuGENE® HD Transfection Reagent according to the manufacturer's instructions. A Renilla luciferase control plasmid, pRL-CMV (Promega Co.), was co-transfected as the internal control for determining transfection efficiency. Luciferase activities were determined using a Dual Luciferase® Reporter Assay System (Promega Co.) and the VICTOR Multilabel Plate Reader.

Measurement of intracellular ROS levels

BV-2 microglial cells were seeded in six-well plates and allowed to proliferate to 80% confluence. The cells were then stained with a general oxidative stress indicator (CM-H2DCFDA, a fluorescent probe). After 30 mins of incubation, the cells were harvested and suspended in PBS. Fluorescence intensity was analyzed using a flow

cytometer (Beckman Coulter FC500, Pasadena, CA, USA). The data were quantified using CXP 2.0. At least 10,000 cells were evaluated for each run.

siRNA transfection

BV-2 microglial cells were transfected with control siRNAs or mouse *HO-1*, *NQO-1*, *Nrf2*, and *AMPK* siRNA using the X-tremeGENE siRNA Transfection Reagent according to the manufacturer's protocol. In brief, BV-2 microglial cells were incubated with control siRNA or mouse *HO-1*, *NQO-1*, *Nrf2*, or *AMPK* siRNA in serum-free Gibco™ Opti-MEM™ media (Thermo Fisher Scientific, Inc). The specific siRNA-transfected cells were prepared, and the protein expression of HO-1, NQO-1, Nrf2, and AMPK were analyzed by western blot analysis.

Western blot analysis

The total protein samples of microglia and BV-2 microglial cells were obtained using a radioimmunoprecipitation assay buffer (Thermo Fisher Scientific, Inc.) with a protease inhibitor cocktail (Roche Applied Science, Indianapolis, IN, USA). The nuclear protein samples were extracted using the NE-PER™ Nuclear and Cytoplasmic Extraction Kit (Thermo Fisher Scientific Inc.). Extractions were performed strictly according to the manufacturer's protocol. The samples were quantified using the Bio-Rad protein assay kit. Samples were separated by SDS-PAGE and transferred onto polyvinylidene difluoride membranes. Blotted membranes were incubated with primary antibodies, followed by visualization using a horseradish peroxidase-conjugated secondary antibody. Peroxidase activity was detected by SuperSignal Western Blot Enhancer (Thermo Fisher Scientific Inc.). The blots were examined by ImageQuant 350 analyzer (Amersham Biosciences).

Statistical analysis

All results are expressed as mean±SD. Each experiment was performed a minimum of three times. Statistically significant differences were assessed using one-way ANOVA followed by Dunn's post-hoc test. $P<0.05$ (significant) or $P<0.01$ (highly significant) were considered as statistically significant levels.

Results and discussion

Optimization of ES-GNs through antioxidant activity of ES extract

ES extract used to synthesize gold nanoparticles synthesis was analyzed for its total phenolic and flavonoid

content, reducing power potential, and antioxidant activity (by ABTS and DPPH assays). The total phenolic content of ES extract was 287.9 µg gallic acid equivalents/g. The flavonoid content of ES extract was 92.7 µg quercetin equivalents/g. Reducing power potential of ES extract was in the range of 3.78 µg ascorbic acid equivalents/g. Furthermore, ES extract (0.1–1 mg/mL) exhibited DPPH and ABTS radical scavenging activity (10–80%) (Figure 1A and B). These results may be due to the presence of different antioxidant compounds. This finding could be related to the results of reducing power potential, total phenolic and flavonoid content, and antioxidant activity of ES extract, suggesting that reducing power potential, high phenolic and flavonoid content, and antioxidant activity of ES extract could provide an advantage in reducing, capping, and stabilizing of ES-GNs. This is in-line with several research papers suggesting that higher phenolic and flavonoid content are also responsible for providing anti-neuroinflammatory properties. For the green synthesis of gold nanoparticles, ES extract was incubated with chloroauric acid solution. As a result, the light yellow color of ES extract changed to a ruby red color by reduction of chloroauric acid solution. The appearance of ruby red color indicated the formation of gold nanoparticles, which was due to the excitation of surface plasmon vibrations in ES-GNs. Next, the synthesis of ES-GNs was confirmed by UV-Vis spectrophotometry at wavelengths in the range of 300–800 nm (Figure 1C and D). The spectrum of ES extract showed no peaks but that of ES-GNs showed a characteristic absorption peak at a wavelength of approximately 528 nm, which was attributed to surface plasmon resonance. For ES-GNs, synthesis was successfully confirmed directly in the suspension with purified gold nanoparticles. Reaction parameters of optimization of gold nanoparticles, such as ES extract concentration, chloroauric acid solution concentration, and reaction times should be considered to appraise the possibilities for quick and simplified purification of gold nanoparticles. ES extract concentration demonstrated that 1 mg/mL of ES extract was optimal for economic synthesis of ES-GNs (Figure 1E). Time optimization studies revealed that 4 mins were required for ES-GN formation (Figure 1F). Chloroauric acid solution optimization studies revealed that 1 µM chloroauric acid solution was required for its complete reduction to ES-GNs (Figure 1G). Thus, the optimal conditions were identified for ES-GNs green synthesis with respect to ES extract concentration,

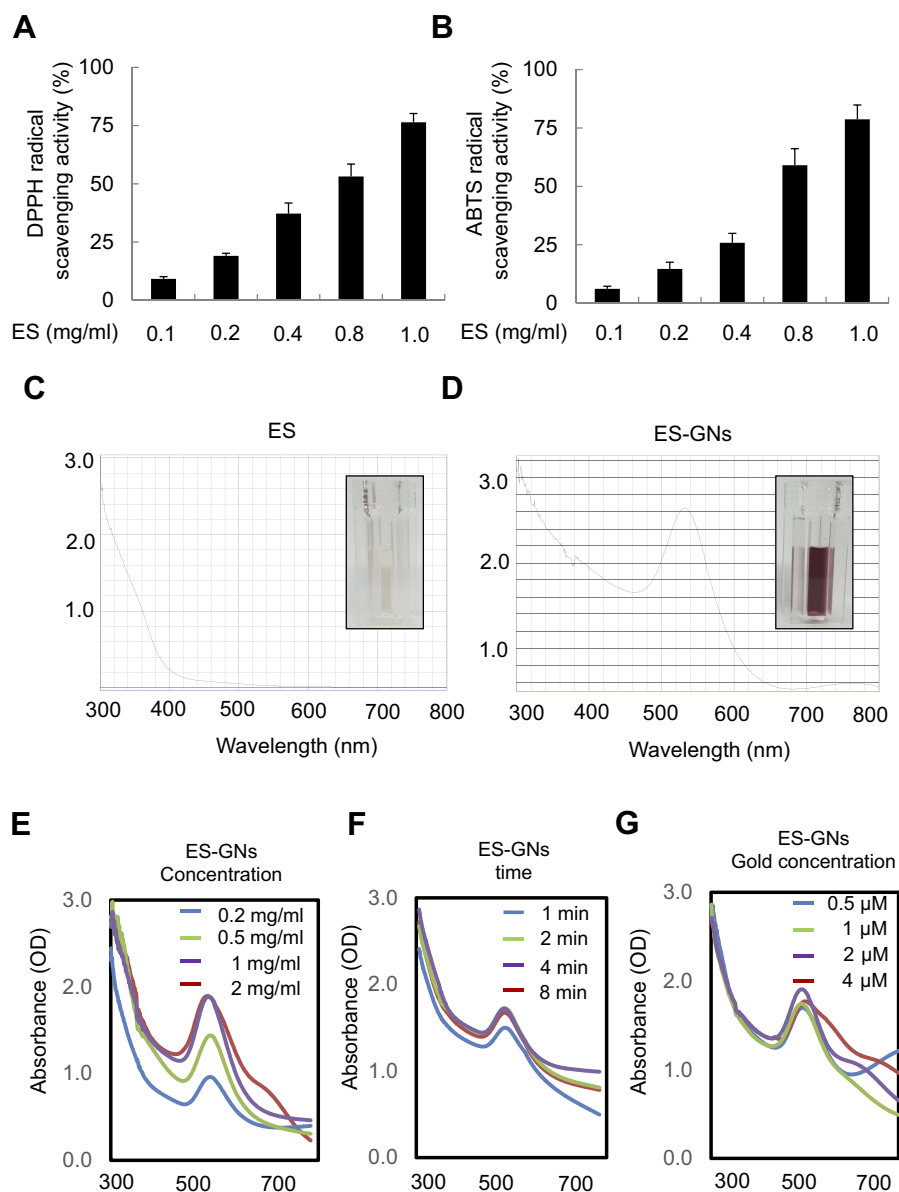


Figure 1 Reducing power potential and antioxidant activity of ES extract and optimization of ES-GNs. DPPH radical scavenging activity (**A**) and ABTS radical scavenging activity (**B**) of ES extract. UV-Vis spectroscopy analysis of ES extract (**C**) and green-synthesized ES-GNs (**D**). Optimization of ES extract concentration (**E**), gold(III) chloride (chloroauric acid) solution concentration (**F**), and reaction times (**G**) for ES-GN production.

Abbreviations: ES, *Ephedra sinica* Stapf; DPPH, 2,2-diphenyl-1-picrylhydrazyl; ABTS, 2,2'-azino-bis (3-ethylbenzothiazoline-6-sulphonic acid); ES-GNs, ES extract-gold nanoparticles; UV-Vis, ultraviolet-visible.

reaction time, and chloroauric acid solution concentration, resulting in the highest yield and minimal agglomeration.

DLS, HR-TEM, and EDS analysis of ES-GNs

DLS analysis was performed to study the size distribution and zeta potential of ES-GNs and to determine the hydrodynamic diameter and available surface charge to be electrostatically stabilized and resistant to spontaneous

aggregation. For ES-GNs, the hydrodynamic size was 57.6 ± 3.07 nm with a polydispersity index (PDI) value of 0.34 (Figure 2A). The relative PDI value is indicative of size distribution in ES-GNs. The zeta potential was -24.6 ± 0.84 mV with a single peak. High negative zeta potential values indicated the presence of a repulsive force for electrostatic stabilization (Figure 2B). Commonly, the hydrodynamic size is higher than that measured from the HR-TEM images as the hydrodynamic size includes the hydration layer in addition with

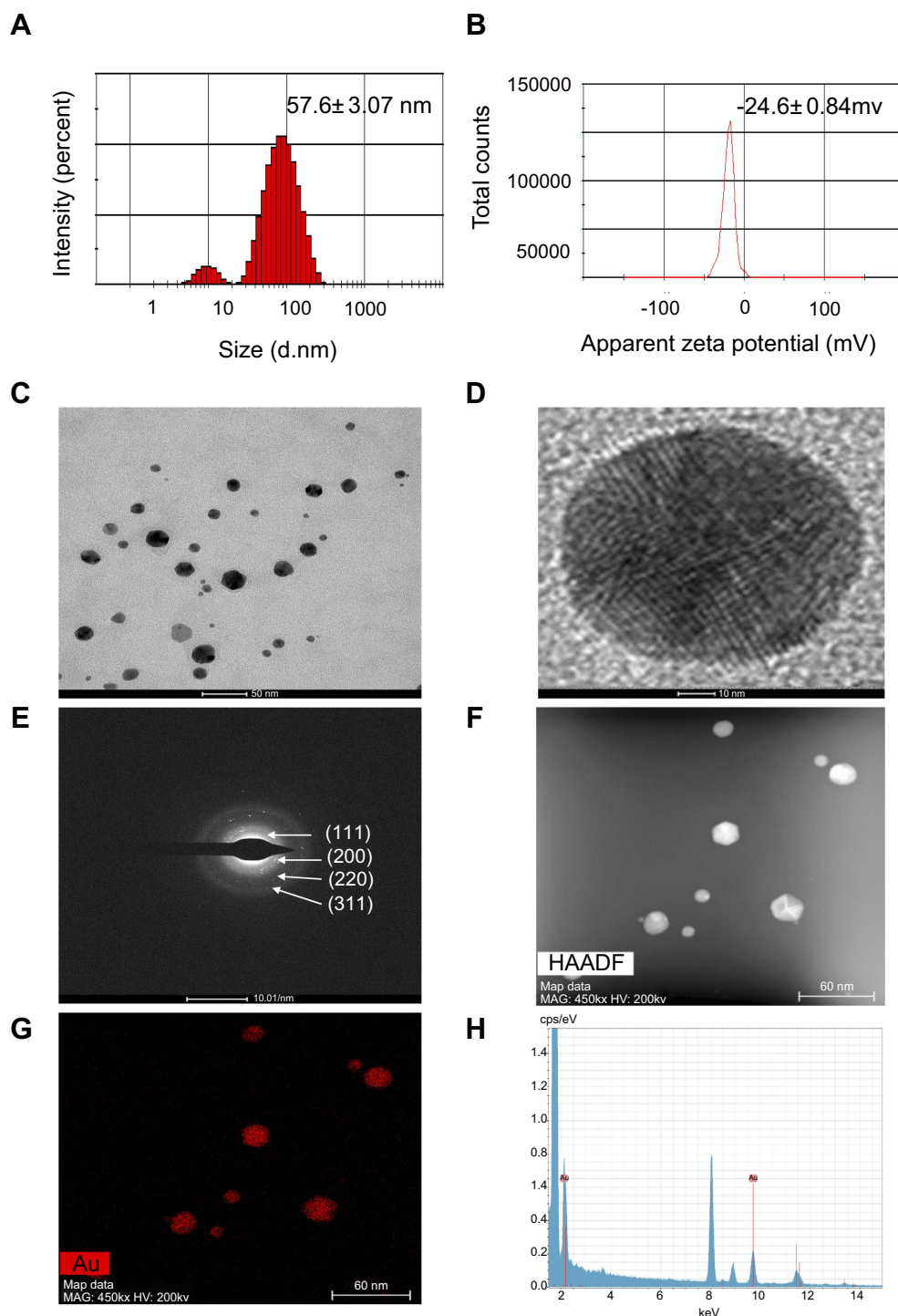


Figure 2 DLS and HR-TEM images of ES-GNs showing the SAED pattern, HAADF, and EDS. The hydrodynamic size (**A**) and zeta potential (**B**) of ES-GNs were determined by DLS. (**C–D**) Particle shape of ES-GNs was confirmed by low- and high-magnification images and HR-TEM images. The SAED pattern (**E**), HAADF image (**F, G**), and EDS analysis (**H**) of ES-GNs.

Abbreviations: DLS, dynamic light scattering; HR-TEM, high-resolution transmission electron microscopy; SAED, selected area electron diffraction; HAADF, high-angle annular dark field; EDS, energy dispersive spectroscopy.

the ES extract on the surface. HR-TEM images confirmed the presence of spherical or hexagonal-shaped ES-GNs, with the approximate size of 35.04 ± 4.02 nm (Figure 2C and D). The face-centered cubic crystal

structure of ES-GNs was also indicated by the bright circular spots in the selected area electron diffraction pattern corresponding to lattice planes of Bragg's reflection (111), (200), (220), and (311) planes, which indexed

d-spacings of 0.24, 0.22, 0.15, and 0.12, respectively (Figure 2E). High-angle annular dark field-TEM further confirmed the presence of gold composite nanoparticles (Figure 2F and G). Moreover, this was confirmed by EDS analysis, indicating the presence of elemental gold peak, which are the green synthesized gold nanoparticles from ES extract. The optical adsorption peak of ES-GNs was confirmed at nearly 2.20, 9.75, and 11.63 keV, thereby confirming the presence of gold (Figure 2H).

XRD and FT-IR analysis of ES-GNs

The XRD pattern of ES-GNs displayed characteristic peaks that were in agreement with those of well-crystallized gold pattern. Based on the XRD spectrum, the peaks were presented at 37.77°, 43.74°, 64.50°, and 77.33°, which were indicative of (111), (200), (220),

and (311) planes of face-centered cubic structure for gold nanoparticles, respectively. The diffraction intensity of the (111) planes was intensely strong compared to that of the (200), (220), and (311) planes, indicating that the (111) plane was the main crystal orientation of ES-GNs. These results suggest that the reducing factors from ES extract specially adsorbed lower surface energy of the (111) plane and facilitated the growth of the Au crystal facets in this plane (Figure 3A and B). FT-IR spectroscopy analysis is effective for determining the quantitative elemental composition of ES extract adsorbed on ES-GN surface involved in ES-GN synthesis. FT-IR spectrum of ES extract and ES-GNs suggested an extensive resemblance between both the samples. FT-IR spectra of ES extract and ES-GNs were characterized by the O–H band at 3,413.03 and

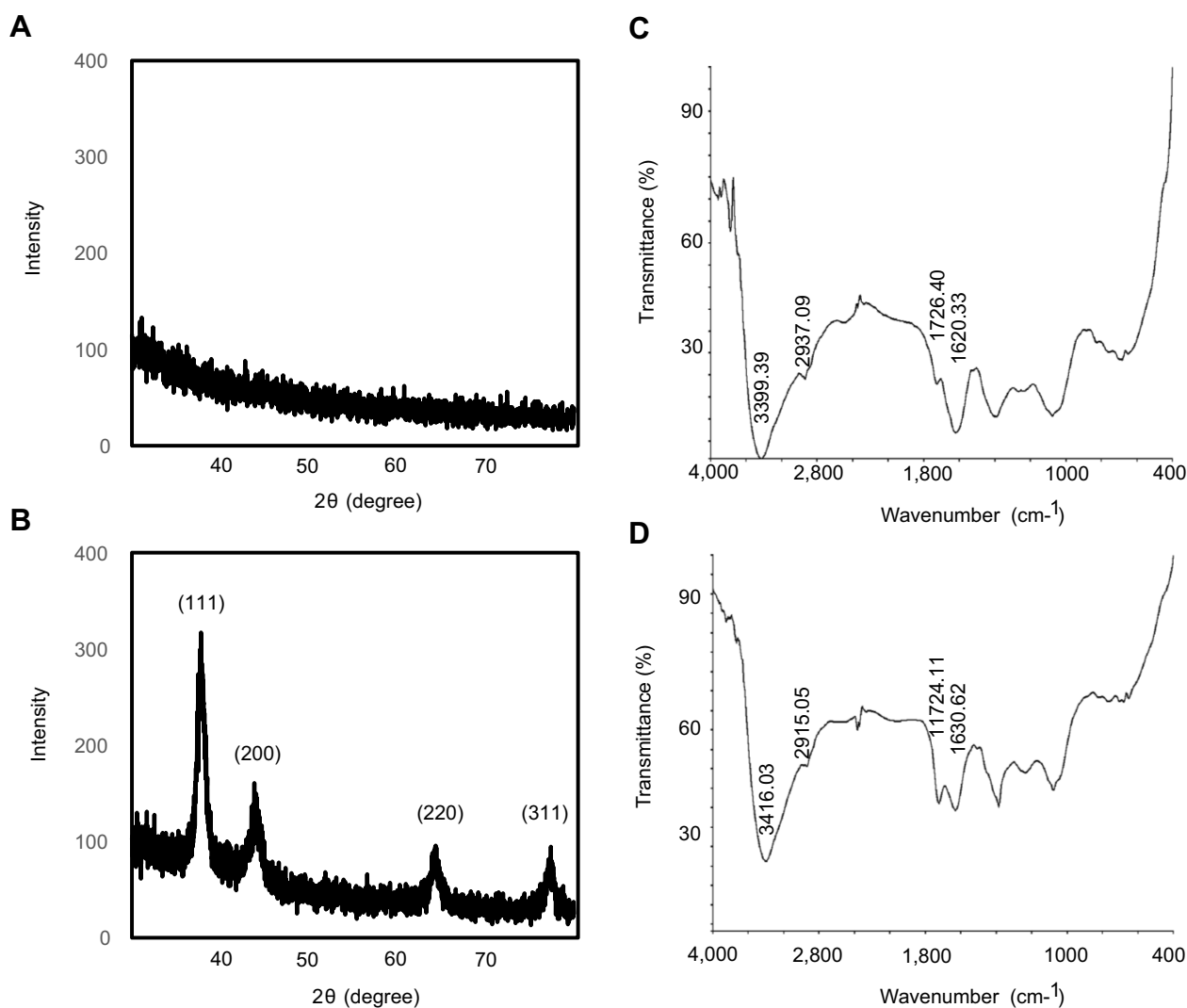


Figure 3 XRD and FT-IR spectra of ES-GNs. XRD patterns of ES extract (**A**) and synthesized ES-GNs (**B**). FT-IR spectra of ES extract (**C**) and synthesized ES-GNs (**D**). **Abbreviations:** XRD, X-ray diffraction; FT-IR, Fourier transform-infrared spectroscopy.

3,399.39 cm^{-1} respectively, and C–H stretching between 2,937.09 and 2,915.05 cm^{-1} respectively, was also observed. Moreover, C=C bonds stretching between 1,726.40 and 1,724.11 cm^{-1} and N–H bending of 1620.33 and 1630.62 cm^{-1} were detected in the two samples, respectively (Figure 3C and D), clearly indicating that the phenolic compounds of ES extract were likely to be accountable for reduction to ES-GNs.

ES-GNs exhibited no cytotoxic effect and reduced pro-inflammatory cytokine levels and ROS production

Mouse primary microglia and immortal BV-2 mouse microglial cells exhibit similar neuroinflammatory responses. Therefore, neuroinflammation-related drug research on primary microglia and BV-2 microglial cells is normally performed to elucidate neurodegenerative disorders characterized by chronic neuroinflammatory responses.⁴² To investigate cell viability and cytotoxicity effects of ES-GNs on primary microglia and BV-2 microglia cells, cell viability was determined by performing MTT assay at various concentrations of ES-GNs and ES extracts (40 $\mu\text{g}/\text{mL}$). ES-GN treatment did not significantly alter microglia viability (Figure 4A and B). LDH was investigated to confirm whether ES-GNs induced cytotoxicity in primary microglia and BV-2 microglia cells. The results demonstrated that ES-GNs and ES extracts exhibited no cytotoxic effects (Figure 4C and D). According to MTT and LDH assay results, subsequent experiments of ES-GNs and ES extracts with primary microglia and BV-2 microglial cells were performed at concentrations up to 20 $\mu\text{g}/\text{mL}$. LPS, a principal endotoxin of the outer membrane of Gram-negative bacteria, which stimulates expression of pro-inflammatory cytokines and mediators via TLR4 binding, activated a high number of intracellular downstream signaling pathways. Moreover, LPS also induced pro-inflammatory cytokines, such as TNF- α , IL-1 β , and IL-6, in microglia. These pro-inflammatory cytokines play fundamental roles in various neuroinflammation-mediated neurodegenerative diseases.⁴³ We next investigated TNF- α , IL-1 β , and IL-6 inhibition effect of ES-GNs in primary microglia and BV-2 microglial cells stimulated with LPS by ELISA. We confirmed that ES-GNs significantly downregulated the production of pro-inflammatory cytokines TNF- α , IL-1 β , and IL-6. Furthermore, ES-GNs per se had no significant effect

on TNF- α , IL-1 β , and IL-6 production. ES extract also did not significant inhibitory effect on these productions (Figure 4E and F). ROS are major factors involved in promoting neuroinflammatory responses, and their over-production increases LPS-stimulated microglia.²⁹ We analyzed ROS production in primary microglia and BV-2 microglial cells using a flow cytometer. We determined that ROS production was strongly induced in LPS-stimulated microglia. However, we found that ES-GN pre-treatment reduced ROS production in LPS-stimulated primary microglia and BV-2 microglial cells. There was no significant difference in ROS production in the control and ES-GNs alone without LPS stimulation groups. ES extract also did not significant inhibitory effect on ROS production (Figure 4E and F). These results suggest that ES-GNs exhibited inhibitory effects on pro-inflammatory cytokines and ROS production in LPS-stimulated primary microglia and BV-2 microglial cells.

ES-GNs suppressed neuroinflammatory factor via NF- κB , JAK/STAT, MAPK, and PLD pathways

iNOS and COX-2 were also involved in neuroinflammation-induced progression of neurodegenerative diseases. The overexpression of iNOS and COX-2 in microglia caused neurotoxicity by producing excessive NO and PGE₂, and knockdown system of INOS and COX-2 showed neuroprotective properties in microglia and mouse models. Furthermore, LPS-induced NO and PGE₂ production and increased expression of iNOS and COX-2 in microglia are associated with neurodegenerative diseases.³⁰ This is in-line with published results suggesting that overactivation and overexpression of iNOS and COX-2 by microglia has various deleterious effects on neuronal constituents. To investigate iNOS and COX-2 enzymatic activity, Griess reagent and ELISA kits were used to detect the production of NO and PGE₂ in primary microglia and BV-2 microglial cells. The results showed that in the LPS-stimulated group, a significant increase in the production of NO and PGE₂ was observed compared to that in the control group, whereas ES-GNs dose-dependently inhibited LPS-stimulated production of NO and PGE₂ in primary microglia and BV-2 microglial cells. ES extract did not significant inhibitory effect on these productions (Figure 5A and B). To investigate whether inhibitory effects of NO and PGE₂ by ES-GNs were controlled at

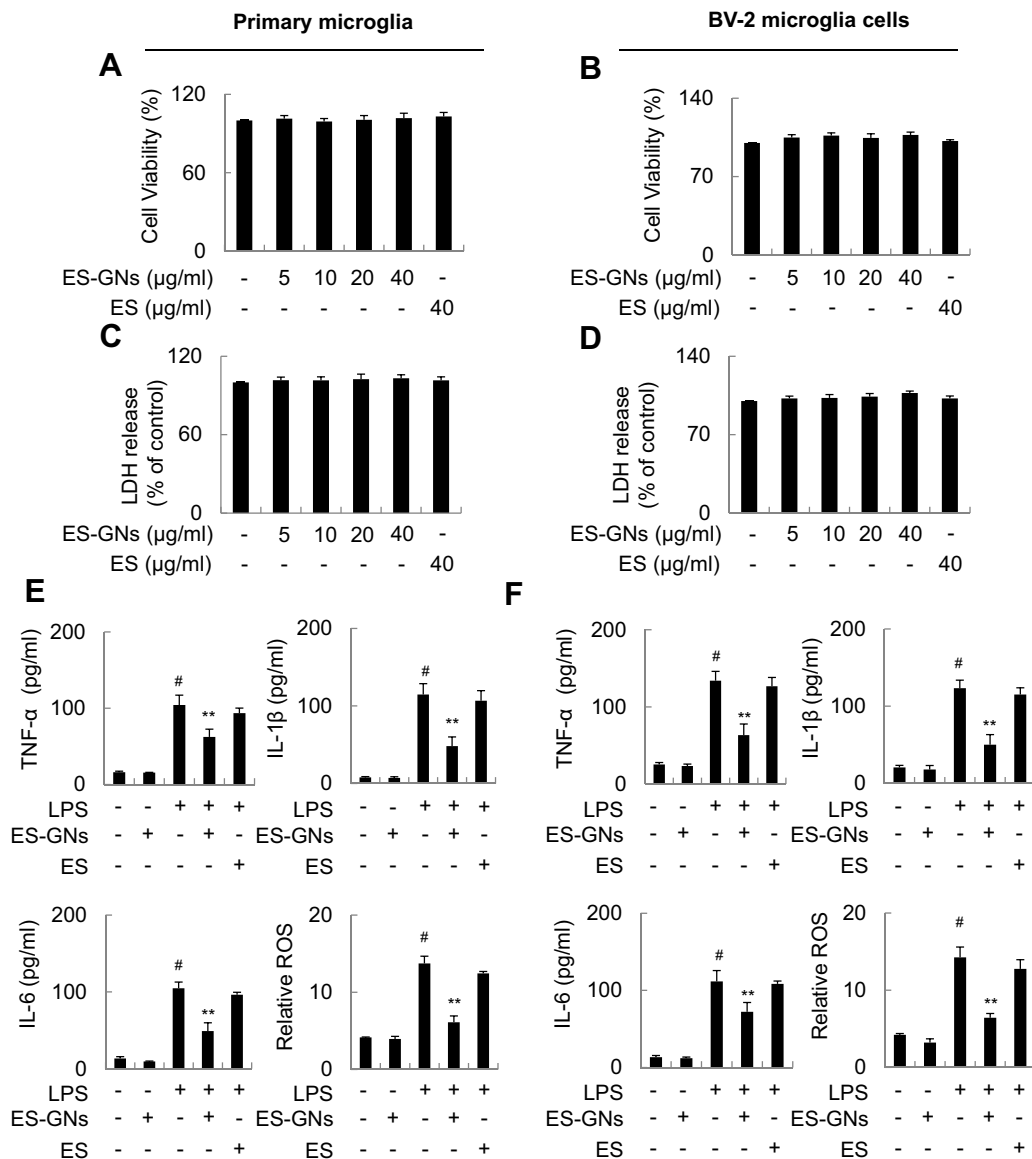


Figure 4 Effect of ES extract and ES-GNs on microglia viability and pro-inflammatory cytokine production. Primary microglia (**A**) and BV-2 microglia cell viability (**B**) were determined using the MTT assay. Primary microglia (**C**) and BV-2 microglia cell cytotoxicity (**D**) were analyzed using the LDH assay. (**E, F**) The production of TNF- α , IL-1 β , and IL-6 in the culture media was analyzed using a commercial ELISA kit. ROS content was determined using CM-H₂DCFDA. # $P < 0.01$ relative to the control group. * $P < 0.05$ and ** $P < 0.01$ relative to the LPS-treated group.

Abbreviations: ES, Ephedra sinica; LDH, lactate dehydrogenase; TNF- α , tumor necrosis factor- α .

the mRNA level, promoter activity, and protein expression, we performed real-time PCR, luciferase assay, and western blotting, respectively, for iNOS and COX-2. The mRNA level, promoter activity, and protein expression of iNOS and COX-2 increased significantly in response to LPS, whereas ES-GNs inhibited these effects in a dose-dependent manner. ES extract did not significant inhibitory effect on these protein expression (Figure 5C–G). There was no significant difference in iNOS and COX-2 enzymatic activity and expression level in the control and ES-GNs alone without LPS stimulation groups. Numerous

previous studies have revealed that a high number of intracellular signaling pathways, such as IKK- α/β , NF- κ B, JAK/STAT, ERK-1/2, p38 MAPK, JNK, and PLD signaling pathways, play an essential role in the regulation of neuroinflammation responses during chronic activated microglia. NF- κ B, an important transcription factor, plays a key role by regulating neuroinflammatory responses.^{20,23} Therefore, phosphorylation level, nuclear translocation, and promoter binding activity were determined to evaluate the activation of IKK- α/β , NF- κ B, JAK/STAT, ERK-1/2, p38 MAPK, JNK, and PLD in LPS-stimulated BV-2

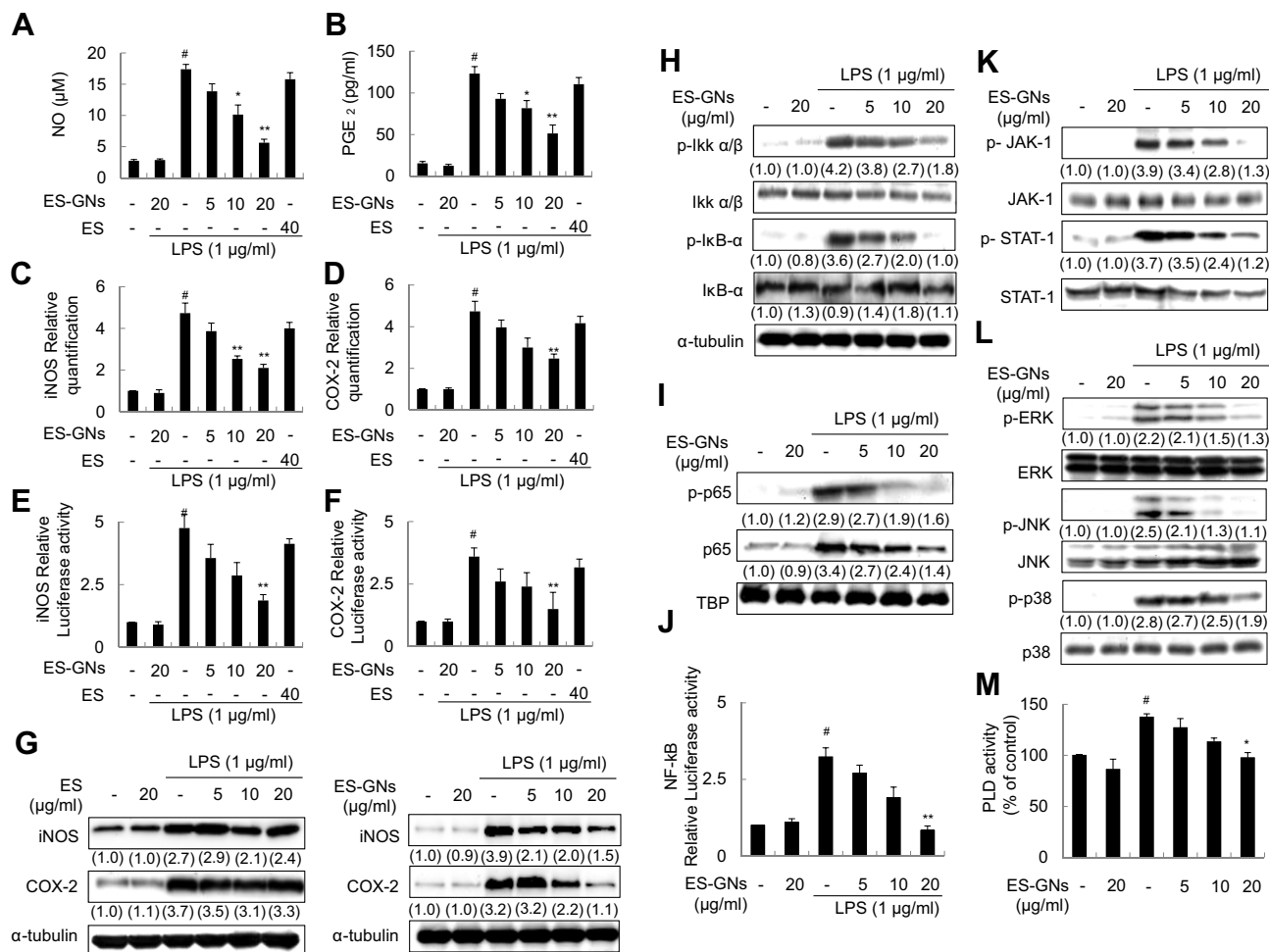


Figure 5 Effect of ES-GNs on iNOS and COX-2 activity via the IKK- α/β , NF- κ B, JAK/STAT, ERK-1/2, p38 MAPK, JNK, and PLD signaling pathways in BV-2 microglia cell. NO content (**A**) was measured using the Griess reaction. PGE₂ (**B**) was measured using a commercial ELISA kit. The relative mRNA levels encoding iNOS (**C**) and COX-2 (**D**) were determined by real-time RT-PCR. Dual luciferase assay was performed to evaluate iNOS (**E**) and COX-2 (**F**) promoter activity. (**G**) Western blotting and semi-quantitative analysis were performed to estimate iNOS, COX-2, and α -tubulin protein levels. (**H**) Western blot analysis and semi-quantitative analysis were performed to evaluate the protein expression of p-IKK- α/β , IKK- α/β , p-I κ B- α , I κ B- α , and α -tubulin. (**I**) Western blot analysis and semi-quantitative analysis were performed to evaluate the protein expression of NF- κ B p65, p-NF- κ B p65, and TBP. (**J**) Dual luciferase assay was performed to evaluate NF- κ B p65 promoter binding activity. (**K**) Western blotting and semi-quantitative analysis were performed to estimate protein levels of p-JAK-1, p-STAT-1, JAK-1, and STAT-1. (**L**) Western blotting and semi-quantitative analysis were performed to estimate the protein expression of p-ERK, p-JNK, p-p38, ERK, JNK, and p38. (**M**) Amplex Red PLD assay kit was used to estimate the PLD activity. # $P < 0.01$ relative to the control group. * $P < 0.05$ and ** $P < 0.01$ relative to the LPS-treated group.

Abbreviations: NO, nitrite; PGE₂, prostaglandin E₂; iNOS, inducible nitric oxide synthase; COX-2, cyclooxygenase; p-, phosphorylated; IKK, I κ B kinase; TBP, TATA-binding protein; JAK, Janus-activated kinase; STAT, signal transducers and activators of transcription; ERK, extracellular signal-regulated kinase; JNK, c-JUN N-terminal kinase; PLD, phospholipase D.

microglial cells. As indicated, compared with the control, LPS strongly increased the phosphorylation of IKK- α/β and NF- κ B p65. However, when the LPS-stimulated BV-2 microglial cells were pre-treated with ES-GNs, ES-GNs reduced the phosphorylation of IKK- α/β and NF- κ B p65 (Figure 5H and I). We further confirmed that nuclear translocation and promoter binding activity of NF- κ B p65 were significantly attenuated by ES-GNs treatment in LPS-stimulated BV-2 microglial cells (Figure 5I and J). These results also showed that ES-GNs dose-dependently suppressed the phosphorylation of JAK-1 and STAT-1 in LPS-stimulated BV-2 microglial cells (Figure 5K).

Similarly, phosphorylation of ERK-1/2, p38 MAPK, and JNK was inhibited by ES-GNs in a concentration-dependent manner in LPS-stimulated BV-2 microglial cells (Figure 5L). PLD is expressed on various immune cells and is significant in the regulation of cytokine production.¹⁶ Thus, we examined whether PLD activity was inhibited by ES-GNs using the Amplex Red PLD assay kit. LPS stimulation increased PLD activity, whereas treatment with ES-GNs inhibited PLD activity in LPS-stimulated BV-2 microglial cells (Figure 5M). ES-GNs alone had no significant effect on IKK- α/β , NF- κ B, JAK/STAT, ERK-1/2, p38 MAPK, JNK, and PLD activation.

These findings suggested that ES-GNs exhibited anti-neuroinflammatory properties by inhibiting the activation of IKK- α/β , NF- κ B, JAK/STAT, ERK-1/2, p38 MAPK, JNK, and PLD signals in LPS-stimulated BV-2 microglial cells.

AMPK and NRF2/ARE activation mediated ES-GNs-induced anti-neuroinflammatory properties

HO-1 and NQO1 are major antioxidant response factors in neuroinflammatory responses and are an important cellular mechanism to eliminate pro-inflammatory mediators and

cytokines.⁴⁴ Consistent with previous studies, we found that ES-GNs significantly induced HO-1 and NQO1 protein expression levels in LPS-stimulated BV-2 microglial cells (Figure 6A and D). To further investigate the impact of HO-1 and NQO1 knockdown on anti-neuroinflammatory properties of ES-GNs, we analyzed siRNA of HO-1 or NQO1 in ES-GN treatment by western blotting and iNOS promoter assay in BV-2 microglial cells. Microglia transfected with HO-1 or NQO1 siRNA effectively weakened the expression of HO-1 or NQO1 (Figure 6B and E). Significantly, we found that HO-1- or NQO1-knockdown groups diminished the ES-GNs-induced inhibitory activity of iNOS promoter when compared with

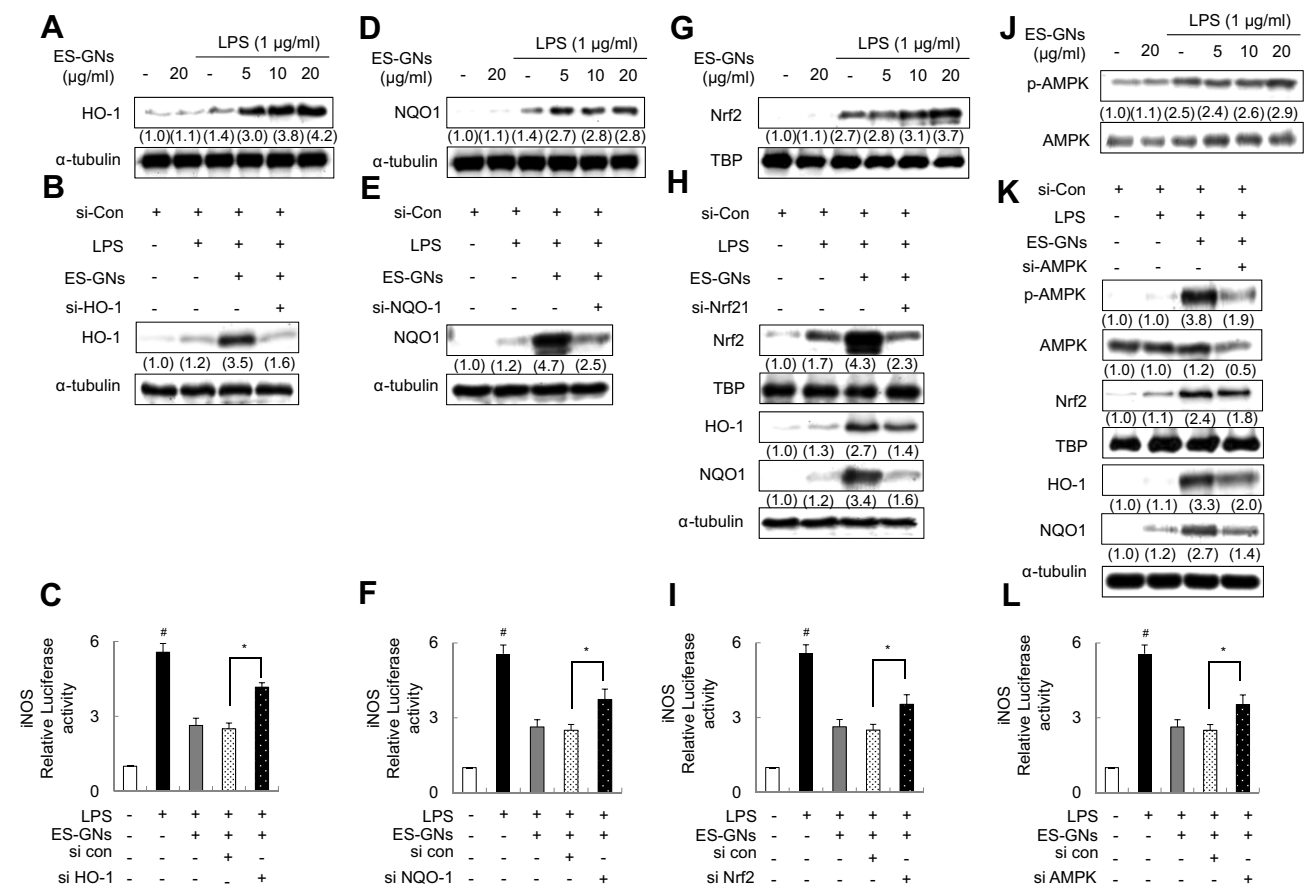


Figure 6 Effect of ES-GNs on anti-neuroinflammatory properties through the AMPK/Nrf2/ARE signaling pathway in BV-2 microglia cell. **(A)** Western blot and semi-quantitative analysis were performed to evaluate the protein expression levels of HO-1 and α -tubulin. **(B)** BV-2 microglia cells were transfected with HO-1 siRNA and treated 20 μ g/mL ES-GNs followed by LPS and analyzed for HO-1 and α -tubulin protein levels. **(C)** BV-2 microglia cells were transfected with HO-1 siRNA and treated 20 μ g/mL ES-GNs followed by LPS and analyzed for iNOS promoter activity. **(D)** NQO1 and α -tubulin protein levels were assessed by western blotting. **(E)** After transfection with NQO1 siRNA were pre-treated with 20 μ g/mL ES-GNs and treated with LPS. NQO1 siRNA system was performed to evaluate the protein expression levels of NQO1 and α -tubulin. **(F)** After transfection with NQO1 siRNA were pre-treated with 20 μ g/mL ES-GNs and treated with LPS. Dual luciferase assay was performed to evaluate iNOS promoter activity in NQO1 siRNA system. **(G)** Western blotting and semi-quantitative analysis were performed to evaluate Nrf2 and TBP protein levels. **(H)** After transfection with Nrf2 siRNA were pre-treated with 20 μ g/mL ES-GNs and treated with LPS. Nrf2 siRNA system was performed to evaluate Nrf2, HO-1, NQO1, TBP, and α -tubulin protein levels. **(I)** After transfection with Nrf2 siRNA were pre-treated with 20 μ g/mL ES-GNs and treated with LPS. Dual luciferase assay was performed to evaluate iNOS promoter activity in Nrf2 siRNA system. **(J)** Western blotting and semi-quantitative analysis were performed to evaluate p-AMPK and AMPK protein levels. **(K)** After transfection with AMPK siRNA were pre-treated with 20 μ g/mL ES-GNs and treated with LPS. AMPK siRNA system was performed to evaluate p-AMPK, AMPK, Nrf2, HO-1, NQO1, TBP, and α -tubulin protein levels. **(L)** After transfection with AMPK siRNA were pre-treated with 20 μ g/mL ES-GNs and treated with LPS. Dual luciferase assay was performed to evaluate iNOS promoter activity in the AMPK siRNA system. # $P < 0.01$ relative to the control group. * $P < 0.05$ and ** $P < 0.01$ relative to the LPS-treated group.

Abbreviations: HO-1, heme oxygenase-1; NQO1, NAD(P)H dehydrogenase1; Nrf2, nuclear erythroid 2-related factor 2; TBP, TATA-binding protein; si, small interfering; AMPK, AMP-activated protein kinase.

transfection with control siRNA in LPS-stimulated BV-2 microglial cells (Figure 6C and F). Nrf2 regulates an array of biological processes, including neuronal homeostasis and anti-neuroinflammatory responses as well as its downstream proteins HO-1 and NQO1.⁴⁴ It was observed that nuclear accumulation of Nrf2 increased significantly following treatment with ES-GNs in LPS-stimulated BV-2 microglial cells (Figure 6G). To further analyze the possible relationship between ES-GNs-induced Nrf2 signal activation and anti-neuroinflammatory properties, we used Nrf2-specific siRNA to silence Nrf2. As shown in Figure 6H, ES-GNs-induced Nrf2 activation and HO-1 or NQO1 expression were blocked in the Nrf2-silenced group. Interestingly, in the Nrf2-silenced group, ES-GNs were ineffective against LPS-stimulated iNOS promoter activity in BV-2 microglial cells (Figure 6I). To elucidate the upstream regulator of ES-GNs-mediated Nrf2/ARE activation, we investigated the activation of AMPK, which regulates cellular metabolic balance and reduces abnormal inflammatory responses.²⁸ The results showed that ES-GN treatment significantly increased the phosphorylation of AMPK in LPS-stimulated BV-2 microglial cells, whereas ES-GNs alone exhibited no effects on AMPK phosphorylation (Figure 6J). Therefore, we made an assumption that ES-GNs exhibited anti-neuroinflammatory properties via activating the AMPK-mediated Nrf2/ARE signal in LPS-stimulated BV-2 microglial cells. We also demonstrated that the AMPK-silenced group inhibited the activation of Nrf2 signaling and suppressed the expression of the downstream proteins HO-1 and NQO1 (Figure 6K). Most importantly, the AMPK-silenced group partially abolished the anti-neuroinflammatory properties of ES-GNs (Figure 6L). Based on the above findings, it is reasonable to assume that the AMPK/Nrf2/ARE signal was involved in the anti-neuroinflammatory properties of ES-GNs in LPS-stimulated microglia.

Limitations of the study

The hepatobiliary elimination of gold nanoparticles

As described above, *E. sinica* Stapf extract-capped gold nanoparticles have a great potential in the neuroinflammatory-mediated neurodegenerative diseases. Nonetheless, gold nanoparticles are inescapable to consider side effects on human health. In particular, the hepatobiliary elimination of gold nanoparticles from the liver through bile into the intestine and feces to pharmacological systems has been a matter in question. Characteristic of gold nanoparticles including shape, size, elasticity, and surface

chemistry largely effect their hepatobiliary elimination. Although the several papers for the low toxicity of gold nanoparticles and their efficient elimination by the hepatobiliary system are increasing, clinical studies are still limited because of the lack of knowledge about the consequences of gold nanoparticles as anti-neuroinflammatory agents against neurodegenerative diseases.

The drug delivery using nanoparticle platform and blood–brain barrier (BBB)

In spite of the significance of therapeutics delivery to the brain, the presence of brain–blood barrier is a critical obstacle to brain transporter of drugs. Gold nanoparticles due to their high biocompatibility, size, surface charge, and functionality provide attractive platform to enhance therapeutic delivery into inaccessible regions like the brain, allowing for a wide range of brain-targeting strategies to be employed. Nevertheless, their deficient BBB permeability confers on them only a limited function to transport them to the brain.

The green synthesis of gold nanoparticle

The most usually employed method for the synthesis of gold nanoparticles is the reduction of chemical by a reducing agent in the presence of stabilizing agent. Unfortunately, many reducing agents are capital or energy exhaustive and many toxic chemicals like surfactants or thiol groups are involved. Therefore, synthesis in medicinal plant often gives a cost-effective, clean, and environmentally harmless final product. Green synthesis is one of the best options due to its eco-friendly nature. Nevertheless, the recent studies have yet to fully demonstrate the complex interactions between medicinal plant and gold nanoparticles in which they synthesize.

Conclusion

ES-GNs were synthesized using ES extract and optimized, and their physicochemical characteristics and antioxidant capacity were determined. To the best of our knowledge, this is the first report indicating that ES-GNs exhibit anti-neuroinflammatory properties in LPS-stimulated microglia. ES-GNs can decrease the levels of pro-neuroinflammatory cytokines and mediators, which results in amelioration of neurodegenerative disorders. Further, ES-GNs exhibited anti-neuroinflammatory properties by decreasing ROS levels in microglia. Mechanistic insights indicated that ES-GNs downregulated the IKK- α/β , NF- κ B, JAK/STAT, ERK-1/2, p38 MAPK, and JNK signaling

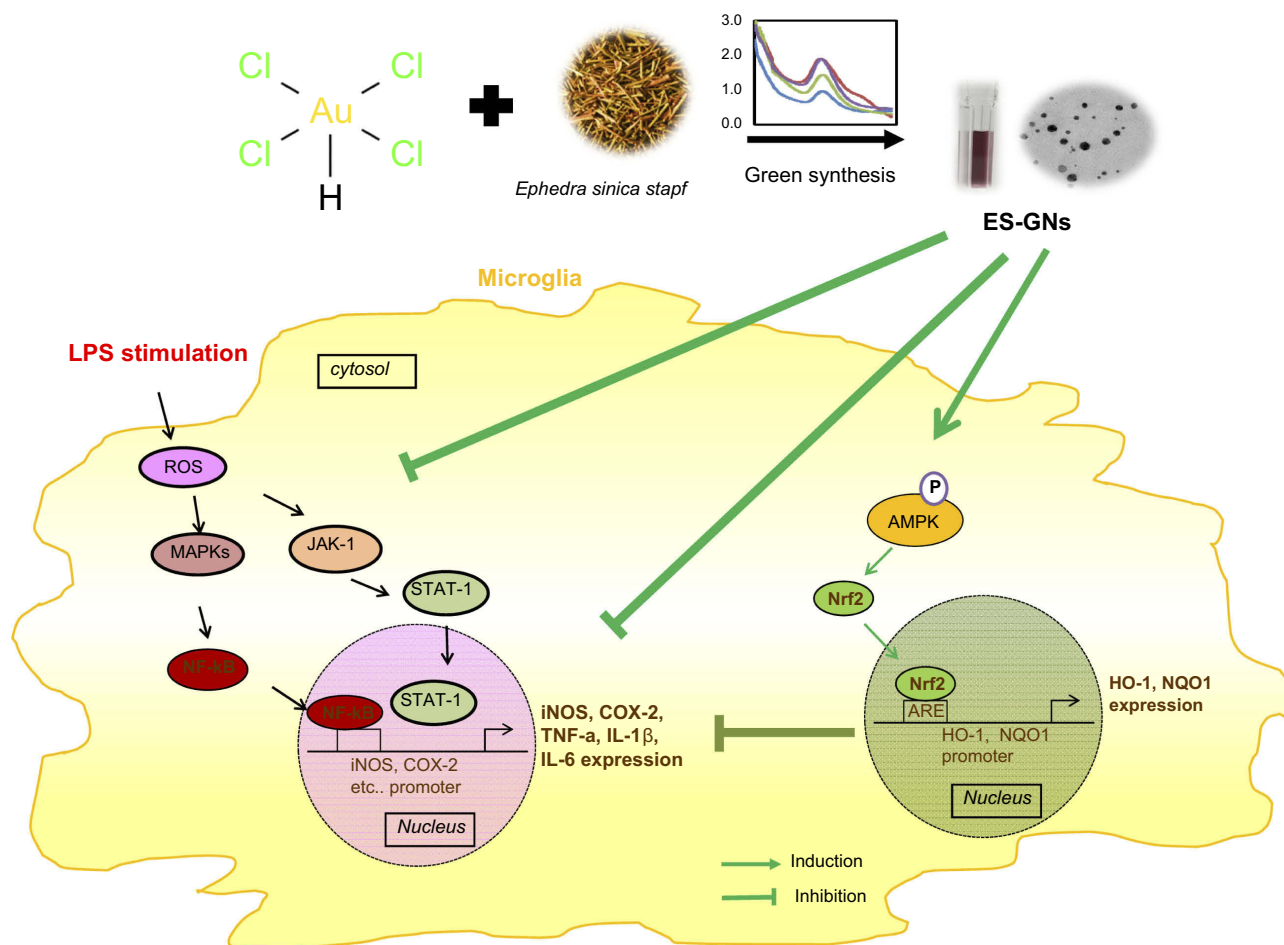


Figure 7 Scheme illustrating the anti-neuroinflammatory properties of ES-GNs in microglia.

Abbreviations: ES-GN, *Ephedra sinica Stapf* extract–gold nanoparticle; TNF- α , tumor necrosis factor- α ; iNOS, Inducible nitric oxide synthase; COX-2, cyclooxygenase-2; p-, phosphorylated; Ikk, I κ B kinase; TBP, TATA-binding protein; JAK, Janus kinase; STAT, signal transducer of activation; MAPKs, Mitogen-activated protein kinases; HO-1, heme oxygenase-1; NQO1, NAD(P)H dehydrogenase 1; Nrf2, nuclear factor erythroid-derived 2-related factor 2; TBP, TATA-binding protein; AMPK, AMP-activated protein kinase.

pathways in LPS-stimulated microglia but upregulated the expression of HO-1 and NQO1 and activation of Nrf2 and AMPK (Figure 7). On the basis of these findings, ES-GNs could serve as a promising anti-neuroinflammatory agent in a therapeutic strategy for treating neuroinflammation-mediated neurodegenerative diseases.

Acknowledgments

This research was supported by the Basic Science Research Program through the National Research Foundation of Korea (NRF), which was funded by the Ministry of Education, Science, and Technology (NRF-2018R1D1A1B07047497 and NRF-2018R1D1A3B07047983). This work was supported by the Technological R&D Program (S2495715) funded by the Ministry of SMEs and Startups (MSS, Korea).

Disclosure

The authors report no conflicts of interest in this work.

References

- Ahn S, Singh P, Jang M, et al. Gold nanoflowers synthesized using *Acanthopanax* cortex extract inhibit inflammatory mediators in LPS-induced RAW264.7 macrophages via NF- κ B and AP-1 pathways. *Colloids Surf B Biointerfaces*. 2017;160:423–428. doi:10.1016/j.colsurfb.2017.09.053
- Abbai R, Mathiyalagan R, Markus J, et al. Green synthesis of multifunctional silver and gold nanoparticles from the oriental herbal adaptogen: siberian ginseng. *Int J Nanomedicine*. 2016;11:3131–3143. doi:10.2147/IJN.S108549
- Duan H, Wang D, Li Y. Green chemistry for nanoparticle synthesis. *Chem Soc Rev*. 2015;44(16):5778–5792. doi:10.1039/c4cs00363b
- Elia P, Zach R, Hazan S, Kolusheva S, Porat Z, Zeiri Y. Green synthesis of gold nanoparticles using plant extracts as reducing agents. *Int J Nanomedicine*. 2014;9:4007–4021. doi:10.2147/IJN.S57343
- Singh P, Ahn S, Kang JP, et al. In vitro anti-inflammatory activity of spherical silver nanoparticles and monodisperse hexagonal gold nanoparticles by fruit extract of *Prunus serrulata*: a green synthetic approach. *Artif Cells Nanomed Biotechnol*. 2018;46(8):2022–2032. doi:10.1080/21691401.2017.1408117

6. Ahn S, Singh P, Castro-Aceituno V, et al. Gold nanoparticles synthesized using Panax ginseng leaves suppress inflammatory – mediators production via blockade of NF-kappaB activation in macrophages. *Artif Cells Nanomed Biotechnol.* 2017;45(2):270–276. doi:10.1080/21691401.2016.1228661
7. Giljohann DA, Seferos DS, Daniel WL, Massich MD, Patel PC, Mirkin CA. Gold nanoparticles for biology and medicine. *Angew Chem Int Ed Engl.* 2010;49(19):3280–3294. doi:10.1002/anie.200904359
8. Dykman L, Khlebtsov N. Gold nanoparticles in biomedical applications: recent advances and perspectives. *Chem Soc Rev.* 2012;41(6):2256–2282. doi:10.1039/c1cs15166e
9. Microbiology: GP. There's gold in them there bugs. *Nature.* 2013;495(7440):S12–S13. doi:10.1038/495S12a
10. Sperling RA, Rivera Gil P, Zhang F, Zanella M, Parak WJ. Biological applications of gold nanoparticles. *Chem Soc Rev.* 2008;37(9):1896–1908. doi:10.1039/b712170a
11. Alam Q, Alam MZ, Mushtaq G, et al. Inflammatory process in Alzheimer's and Parkinson's diseases: central role of cytokines. *Curr Pharm Des.* 2016;22(5):541–548.
12. Kempuraj D, Thangavel R, Natteru PA, et al. Neuroinflammation induces neurodegeneration. *J Neurol Neurosurg Spine.* 2016;1(1):1003.
13. Hu X, Liou AK, Leak RK, et al. Neurobiology of microglial action in CNS injuries: receptor-mediated signaling mechanisms and functional roles. *Prog Neurobiol.* 2014;119–120:60–84. doi:10.1016/j.pneurobio.2014.06.002
14. Theriault P, ElAli A, Rivest S. The dynamics of monocytes and microglia in Alzheimer's disease. *Alzheimers Res Ther.* 2015;7(1). 41-015-0125-2.eCollection 2015. doi:10.1186/s13195-015-0125-2
15. Stamouli EC, Politis AM. Pro-inflammatory cytokines in Alzheimer's disease. *Psychiatriki.* 2016;27(4):264–275. doi:10.22365/jpsych.2016.274.264
16. Gaire BP, Kwon OW, Park SH, et al. Neuroprotective effect of 6-paradol in focal cerebral ischemia involves the attenuation of neuroinflammatory responses in activated microglia. *PLoS One.* 2015;10(3):e0120203. doi:10.1371/journal.pone.0120203
17. Frank-Cannon TC, Alto LT, McAlpine FE, Tansey MG. Does neuroinflammation fan the flame in neurodegenerative diseases? *Mol Neurodegener.* 2009;4:47–1326-4–47. doi:10.1186/1750-1326-4-47
18. Lee JA, Kim JH, Woo SY, et al. A novel compound VSC2 has anti-inflammatory and antioxidant properties in microglia and in Parkinson's disease animal model. *Br J Pharmacol.* 2015;172(4):1087–1100. doi:10.1111/bph.12973
19. Shu Z, Yang B, Zhao H, et al. Tangeretin exerts anti-neuroinflammatory effects via NF-kappaB modulation in lipopolysaccharide-stimulated microglial cells. *Int Immunopharmacol.* 2014;19(2):275–282. doi:10.1016/j.intimp.2014.01.011
20. Su X, Chen Q, Chen W, et al. Mycoepoxydiene inhibits activation of BV2 microglia stimulated by lipopolysaccharide through suppressing NF-kappaB, ERK 1/2 and toll-like receptor pathways. *Int Immunopharmacol.* 2014;19(1):88–93. doi:10.1016/j.intimp.2014.01.004
21. Kang SM, More SV, Park JY, et al. A novel synthetic HTB derivative, BECT inhibits lipopolysaccharide-mediated inflammatory response by suppressing the p38 MAPK/JNK and NF-kappaB activation pathways. *Pharmacol Rep.* 2014;66(3):471–479. doi:10.1016/j.pharep.2013.08.015
22. Santa-Cecilia FV, Socias B, Ouidja MO, et al. Doxycycline suppresses microglial activation by inhibiting the p38 MAPK and NF-kB signaling pathways. *Neurotox Res.* 2016;29(4):447–459. doi:10.1007/s12640-015-9592-2
23. Kim BW, Koppula S, Hong SS, et al. Regulation of microglia activity by glaucocalyxin-A: attenuation of lipopolysaccharide-stimulated neuroinflammation through NF-kappaB and p38 MAPK signaling pathways. *PLoS One.* 2013;8(2):e55792. doi:10.1371/journal.pone.0055792
24. Lee YY, Park JS, Lee EJ, et al. Anti-inflammatory mechanism of ginseng saponin metabolite Rh3 in lipopolysaccharide-stimulated microglia: critical role of 5'-adenosine monophosphate-activated protein kinase signaling pathway. *J Agric Food Chem.* 2015;63(13):3472–3480. doi:10.1021/jf506110y
25. Chen CC, Lin JT, Cheng YF, et al. Amelioration of LPS-induced inflammation response in microglia by AMPK activation. *Biomed Res Int.* 2014;2014:692061.
26. Lee J, Kim S. Upregulation of heme oxygenase-1 expression by dehydrodiconiferyl alcohol (DHCA) through the AMPK-Nrf2 dependent pathway. *Toxicol Appl Pharmacol.* 2014;281(1):87–100. doi:10.1016/j.taap.2014.07.011
27. Mo C, Wang L, Zhang J, et al. The crosstalk between Nrf2 and AMPK signal pathways is important for the anti-inflammatory effect of berberine in LPS-stimulated macrophages and endotoxin-shocked mice. *Antioxid Redox Signal.* 2014;20(4):574–588. doi:10.1089/ars.2012.5116
28. Park SY, Jin ML, Chae SY, et al. Novel compound from Polygonum multiflorum inhibits inflammatory response in LPS-stimulated microglia by upregulating AMPK/Nrf2 pathways. *Neurochem Int.* 2016;100:21–29. doi:10.1016/j.neuint.2016.08.006
29. Jayasooriya RG, Lee KT, Choi YH, Moon SK, Kim WJ, Kim GY. Antagonistic effects of acetylshikonin on LPS-induced NO and PGE2 production in BV2 microglial cells via inhibition of ROS/PI3K/Akt-mediated NF-kappaB signaling and activation of Nrf2-dependent HO-1. *In Vitro Cell Dev Biol Anim.* 2015;51(9):975–986. doi:10.1007/s11626-015-9922-y
30. Park SY, Jin ML, Wang Z, Park G, Choi YW. 2,3,4',5-tetrahydroxystilbene-2-O-beta-d-glucoside exerts anti-inflammatory effects on lipopolysaccharide-stimulated microglia by inhibiting NF-kappaB and activating AMPK/Nrf2 pathways. *Food Chem Toxicol.* 2016;97:159–167. doi:10.1016/j.fct.2016.09.010
31. Krizevski R, Bar E, Shalit O, Sitrit Y, Ben-Shabat S, Lewinsohn E. Composition and stereochemistry of ephedrine alkaloids accumulation in Ephedra sinica Stapf. *Phytochemistry.* 2010;71(8–9):895–903. doi:10.1016/j.phytochem.2010.03.019
32. Huang SK, Lai CS, Chang YS, Ho YL. Utilization pattern and drug use of traditional Chinese medicine, Western medicine, and integrated Chinese-Western medicine treatments for allergic rhinitis under the national health insurance program in Taiwan. *J Altern Complement Med.* 2016;22(10):832–840. doi:10.1089/acm.2015.0080
33. Li L, Li J, Zhu Y, Fan G. Ephedra sinica inhibits complement activation and improves the motor functions after spinal cord injury in rats. *Brain Res Bull.* 2009;78(4–5):261–266. doi:10.1016/j.brainresbull.2008.10.002
34. Oh J, Lee H, Lim H, Woo S, Shin SS, Yoon M. The herbal composition GGEx18 from Laminaria japonica, Rheum palmatum, and Ephedra sinica inhibits visceral obesity and insulin resistance by upregulating visceral adipose genes involved in fatty acid oxidation. *Pharm Biol.* 2015;53(2):301–312. doi:10.3109/13880209.2014.917328
35. Wang Q, Shu Z, Xing N, et al. A pure polysaccharide from Ephedra sinica treating on arthritis and inhibiting cytokines expression. *Int J Biol Macromol.* 2016;86:177–188. doi:10.1016/j.ijbiomac.2016.01.010
36. Yeom MJ, Lee HC, Kim GH, et al. Anti-arthritic effects of Ephedra sinica STAPF herb-acupuncture: inhibition of lipopolysaccharide-induced inflammation and adjuvant-induced polyarthritis. *J Pharmacol Sci.* 2006;100(1):41–50.
37. Aouey B, Samet AM, Fetoui H, Simmonds MSJ, Bouaziz M. Antioxidant, anti-inflammatory, analgesic and antipyretic activities of grapevine leaf extract (Vitis vinifera) in mice and identification of its active constituents by LC-MS/MS analyses. *Biomed Pharmacother.* 2016;84:1088–1098. doi:10.1016/j.biopha.2016.10.033
38. Bahloul N, Bellili S, Aazza S, et al. Aqueous extracts from Tunisian diplotaxis: phenol content, antioxidant and anti-acetylcholinesterase activities, and impact of exposure to simulated gastrointestinal fluids. *Antioxidants (Basel).* 2016;5(2). doi:10.3390/antiox5020012

39. Kumar CS, Loh WS, Ooi CW, Quah CK, Fun HK. Structural correlation of some heterocyclic chalcone analogues and evaluation of their antioxidant potential. *Molecules*. 2013;18(10):11996–12011. doi:10.3390/molecules181011996
40. Oueslati S, Ellili A, Legault J, et al. Phenolic content, antioxidant and anti-inflammatory activities of Tunisian *Diplotaxis simplex* (Brassicaceae). *Nat Prod Res*. 2015;29(12):1189–1191. doi:10.1080/14786419.2014.983505
41. Giulian D, Baker TJ. Characterization of ameboid microglia isolated from developing mammalian brain. *J Neurosci*. 1986;6(8):2163–2178.
42. Kawabori M, Yenari MA. The role of the microglia in acute CNS injury. *Metab Brain Dis*. 2015;30(2):381–392. doi:10.1007/s11011-014-9531-6
43. Luo XL, Liu SY, Wang LJ, et al. A tetramethoxychalcone from *Chloranthus henryi* suppresses lipopolysaccharide-induced inflammatory responses in BV2 microglia. *Eur J Pharmacol*. 2016;774:135–143. doi:10.1016/j.ejphar.2016.02.013
44. Onasanwo SA, Velagapudi R, El-Bakoush A, Olajide OA. Inhibition of neuroinflammation in BV2 microglia by the biflavonoid kolaviron is dependent on the Nrf2/ARE antioxidant protective mechanism. *Mol Cell Biochem*. 2016;414(1–2):23–36. doi:10.1007/s11010-016-2655-8

International Journal of Nanomedicine

Dovepress

Publish your work in this journal

The International Journal of Nanomedicine is an international, peer-reviewed journal focusing on the application of nanotechnology in diagnostics, therapeutics, and drug delivery systems throughout the biomedical field. This journal is indexed on PubMed Central, MedLine, CAS, SciSearch®, Current Contents®/Clinical Medicine,

Journal Citation Reports/Science Edition, EMBase, Scopus and the Elsevier Bibliographic databases. The manuscript management system is completely online and includes a very quick and fair peer-review system, which is all easy to use. Visit <http://www.dovepress.com/testimonials.php> to read real quotes from published authors.

Submit your manuscript here: <https://www.dovepress.com/international-journal-of-nanomedicine-journal>